Sand column impact with a rigid target

S. Park[+], T. Uth[+], N.A. Fleck[+], H.N.G. Wadley* and V.S. Deshpande[+]

[+]*Department of Engineering, Cambridge University,*
Trumpington Street, Cambridge, CB2 1PZ, UK

**Department of Materials Science & Engineering*
University of Virginia, Charlottesville, Va 22903

Abstract

A laboratory-based methodology to launch cylindrical sand slugs at high velocities is developed. The experimental set-up comprises a launcher with a cylindrical cavity and a piston to push out the sand slug. The apparatus is used to launch both dry and fully water saturated sand slugs. High speed photography is used to characterise the evolution of the sand slugs after they are launched. We show that the diameter of the slugs remains unchanged with the sand particles having only an axial velocity component. However, the sand particles have a linear spatial axial velocity gradient which results in the lengthening of the slugs as they travel towards their target. Thus, while the density of the sand slugs decreases with increasing time the linear velocity gradient means that the slugs remain spatially homogenous. The velocity gradient is typically higher in the dry sand slugs compared to the water saturated slugs. The pressure exerted by the slugs on a rigid-stationary target is measured by impacting the slugs against a direct impact Kolsky bar. After an initial high transient pressure, the pressure reduces to a value equal to approximately ρv^2 where ρ is the density of the impacting sand slug and v the particle velocity. This indicates that the loading due to the sand is primarily inertial. The momentum transmitted into the Kolsky bar was approximately equal to the incident momentum of both the dry and water saturated sand slugs. The methodology to launch sand slugs developed here generates well-characterised soil ejecta without the detonation of an explosive. This will permit a laboratory-based experimental investigation of the soil-structure events.

Keywords: *granular material, blast loading, sand-structure interaction.*

1. Introduction

The response of structures to nearby explosions depends upon a variety of factors including the mass, shape and type of explosive, its distance from the explosive and the intervening medium (air, water, soil). While much attention has been devoted to the dynamic response of structures when either water [1, 2, 3] or air [4, 5, 6, 7] resides between the structure and the explosion, the response of structures subjected to loading from a buried explosion has received much less attention.

A number of experimental studies have proposed empirical relations to quantify the deformations of plates subjected to landmine explosions and also have quantified the corresponding impulsive loads; see for example Westine et al. [8] and Neuberger et al [9]. Based on these empirical relations, Morris [10] has proposed a design-for-survivability code for structures subjected to such explosions. A parallel effort also exists to simulate the deformations of structures subjected to the complex loadings created by such explosions. For example, Rimoli et al [11] used a soil model [12] to deduce the impulse applied to structures by explosively driven spherical sand shells and then simulated the ensuing deformation of aluminium monolithic and sandwich plates using finite element calculations. Gruijicic et al. [13] and Wang et al. [14] have presented coupled Eulerian/Lagrangian simulations of landmine explosions and attempted to compare their predictions with blast impulse and plate deformation measurements from Bergeron and Temblay [15] and Foedinger [16]. More recently, Borvik et al. [17] have developed a coupled discrete particle/continuum numerical formulation to simulate the deformation of plates subjected to explosively accelerated spherical sand shells. In all cases, discrepancies exist between measurements and predictions and calibrations are needed before reliable predictions can be made.

The origin of these discrepancies is currently unclear. Two possibilities exist:

(i) The simulations are unable to accurately capture the transfer of momentum from the explosive to the soil during the explosive event.

(ii) The simulations do not accurately capture the interactions between the high velocity soil ejecta and the impacted structure.

An experimental method of generating well-characterised soil ejecta without the detonation of an explosive would help in decoupling the above two issues by enabling us to experimentally investigate the soil-structure interaction phenomena in a more controlled manner. This is the primary aim of this study.

Pingle et al [18] have developed a sand particle impact model and used it to investigate the response of rigid targets to impact by columns of particles of uniform, and axially varied velocity. This rather idealised, but fundamental fluid-structure interaction (FSI) problem is the "sand-blast" analogue to the classical water propagated shock FSI problem studied by Taylor [19]. Liu et al. have recently [20] extended the sand column model to investigate the impact of clamped sandwich and monolithic plates; see Fig. 1a The numerical results indicate that some edge clamped sandwich panel designs suffer significantly smaller deflections than equal mass per unit area monolithic plates of identical span. However, unlike in the water blast situation, the performance benefit in this case was discovered not to be governed by fluid-structure interaction effects, but rather is dominated by the higher bending strength of sandwich plates.

The loading of structures by a column of high velocity sand particles not only provides physical insight into the interaction of sand particles with structures, but also is directly representative of the ejecta created during a landmine explosion. High speed photographs of the sand ejecta from a landmine explosion impacting a V-shaped hull are included in Fig. 1b (modified from Joynt and Williams [21]). The photographs show that the initial soil ejected by the detonation of a buried explosive is well approximated as a cylindrical column of high velocity sand particles. The impact of cylindrical columns of high velocity sand particles against a test structure is therefore a problem of considerable theoretical and experimental interest.

In this study we shall present a laboratory-based method to generate a cylindrical column of high velocity sand particles. This cylindrical column shall subsequently be referred to as a "sand slug". The outline of the paper is as follows. First the experimental apparatus and protocol to generate slugs comprising dry and fully water saturated sand is described. The set-up to measure the loads these slugs exert on rigid and stationary structures is also detailed. The experimental results are then presented in two steps. First the evolution of the sand slugs as they are ejected from the launcher is characterised via observations made from high speed photography and second we report the measured pressures and impulses that arise from the impact of the slugs on a direct impact Kolsky bar. These measurements are used to validate some of the findings of the numerical study by Pingle et al. [18].

2. Experimental protocol

The aim of the experimental study is to develop a methodology to launch cylindrical sand slugs using a laboratory-based gas gun and measure the pressure and momentum imparted by the slugs to a stationary target. We first describe the apparatus used to launch the sand slugs and then proceed to describe the instrumentation employed to measure the pressure and momentum.

2.1 Sand slug launcher

The sand slug launcher comprises a cylindrical cavity wherein the sand slug to be launched is located, a piston that is used to push this sand slug out of the cavity and a high velocity striker that is launched from a gas gun. The striker impacts the piston head and thereby launches the sand slug.

A cross-sectional view of the sand-slug launcher apparatus is sketched in Fig. 2 with all critical dimensions labelled. Unless otherwise stated all components are made from mild steel. We briefly describe each of the components:

(i) *The launcher* primarily comprises a 60 mm thick circular steel plate of diameter 125 mm with a central cylindrical cavity of diameter 12 mm.

(ii) *The piston* that can slide within the cylindrical cavity as shown in Fig. 2 comprises a 70 mm long rod with a piston head that arrests the piston. The front 40mm long segment of the piston rod is of diameter 12 mm such that it slides smoothly within the cylindrical cavity with negligible friction. The rear 30 mm of the rod has been turned down to a diameter of 11 mm so that there is a 1 mm clearance with the cavity wall. This reduction in the diameter was needed to prevent the jamming of the piston inside the cylindrical cavity after the impact of the striker (the high speed impact of the striker results in fattening of the piston rod near the impacted end). In addition a 10 mm thick Aluminium alloy washer of inner diameter 11 mm and outer diameter 25.4 mm (equal to that of the piston head) is located so that it is in contact with the piston head. This washer helps cushion the impact of the piston head against launcher.

(iii) A 10 mm thick *launcher cap* with a central cylindrical cavity also of diameter 12 mm. The launcher cap was bolted onto the front face of the launcher such that cavities of both the launcher and the cap are axially aligned as shown in Fig. 2. The launcher cap serves two purposes: (a) it allows us to locate a front cover that helps maintain the shape of the stationary slug (typically baking paper is used as the front cover as described below) and (b) the front end of the sand slug has to travel 10 mm within the cavity after the slug has been launched: try-and-error experimentation

showed that this extra cavity length helps maintain the shape of the launched sand slug.

(iv) A *striker* of diameter 28.5 mm and mass 0.18 kg that is launched from a gas gun. The striker impacts the piston head centrally and normally at impact velocities in the range of $100\,\text{ms}^{-1}$ - $150\,\text{ms}^{-1}$.

The launcher is bolted to a rigid support frame so that it remains stationary during the impact event.

2.2 Sand slug preparation

The sand slug comprised silica sand with sub-angular particle sizes in the range 150-300 μm; see Fig. 3. The density of solid silica is $2700\,\text{kgm}^{-3}$ while the measured density of the sand compacted in the cylindrical cavity of the launcher was $1650 \pm 50\,\text{kgm}^{-3}$ giving a relative packing density of $\bar{\rho} = 0.61 \pm 0.02$. The sand slug of length $L = 19\,\text{mm}$ and diameter $D = 12\,\text{mm}$ had a sand mass of 3.55g. It was compacted (with a pressure of 60 kPa) into the cylindrical cavity of the launcher in five layers of equal height. The sand slug was held in place by a piece of baking paper covering the mouth of the launcher cavity and the piston pushed firmly against the rear end as shown in Fig. 2. The baking paper was in turn held in place by bolting the launcher cap onto the launcher. The launcher assembly along with the piston was then bolted onto the rigid support frame.

In order to better visualise the deformation of the sand slugs, the sand particles in alternate layers were dyed with water-based black ink. This created a "zebra striped" sand slug as shown in Fig. 2. Two variants of the sand slugs are considered in this study:

(i) Dry sand which was prepared as described above. This is subsequently be referred to as the *dry sand slug*.

(ii) A sand slug with all interstitial spaces filled with water; this fully saturated sand slug is referred to subsequently as the *wet sand slug*. Recall that the sand particles packed to a relative density $\bar{\rho} = 0.61 \pm 0.02$. Thus, after the sand slug was prepared 0.75g (the weight of water required to fill in the 40 vol% interstitial spaces between the particles) of water was poured on the top of the slug and allowed to seep through under the influence of gravity.

2.3 The dynamic test protocol

A circular cylindrical steel striker of diameter 28.5 mm and 0.18 kg mass was fired from

a gas gun so as to impact the head of the piston normally and centrally. The striker was fired from a 28.5 mm diameter bore, 4.5 m long gas gun at velocities of either $v_p = 100\ \mathrm{ms}^{-1}$ or $150\ \mathrm{ms}^{-1}$. The sand slug ejected from the barrel of the sand launcher was visualised using a Phantom V12[1] high speed video camera. Typically, the photographs were taken using an inter-frame time interval of $53\ \mu\mathrm{s}$ with an exposure time of $2\ \mu\mathrm{s}$. The striker imparts a velocity v_o to the piston that was also measured via high speed video photography. For the two values of v_p investigated, the piston velocities were measured to be $v_o = 68\ \mathrm{ms}^{-1}$ and $94\ \mathrm{ms}^{-1}$, respectively. Subsequently, we shall refer to the tests via these piston velocities v_o.

The force (and corresponding impulse) exerted by the sand slug on a nominally rigid and stationary target was measured via an instrumented direct impact Kolsky bar made from a magnesium alloy (grade AZ31). The bar of diameter 22.5 mm and length 890 mm was placed on top of smooth rollers at a stand-off S from the stationary sand slug in the launcher; this stand-off was measured as the distance from the baking paper front cover of the sand slug to impacted end of the Kolsky bar as shown in Fig. 2. Two stand-offs $S = 50$ mm and 150 mm were used in this investigation.

The force exerted by the sand slug was measured using a pair of semiconductor strain gauges[2] mounted diametrically opposite to each other at a 5 bar diameter distance from the impacted end of the Kolsky bar. These gauges were connected in series through a resistor with a fixed resistance $R = 2200\ \Omega$ to a $E = 15$ V DC supply provided by a battery as shown in the circuit diagram in Fig. 4. The change in the potential drop ΔV across the resistor R was measured and related to the longitudinal strain ε (compressive strain is defined as positive) in the Kolsky bar via the relation [22-23]

$$\varepsilon = \frac{\Delta V \left(R + 2R_{\mathrm{SG}}\right)^2}{2R_{\mathrm{SG}} G \left(RE + R\Delta V + 2R_{\mathrm{SG}}\Delta V\right)} \qquad (2.1)$$

where $G = 140$ and $R_{\mathrm{SG}} = 500\ \Omega$ are the gauge factor and resistance of the semi-conductor strain gauges, respectively. The force F_s exerted by the sand slug on the Kolsky bar is then calculated via the relation

$$F_s = E_m A \varepsilon \qquad (2.2)$$

---

[1] Vision Research, 100 Dey Rd. Wayne, NJ, USA.

[2] Model AFP-500-090, Kulite Sensors Limited, Stroudley Rd., Kingsland Business Park, Basingstoke, Hants, RG24 8UG, UK.

where $E_m = 44\,\text{GPa}$ is the Young's modulus of the magnesium alloy and A is the cross-section area of the Kolsky bar. The longitudinal elastic wave speed in the bar was measured to be $4920\,\text{ms}^{-1}$ giving a time-window of $310\,\mu\text{s}$ before elastic reflections from the distal end of the bar complicate the measurement of the force. However, high speed photography (discussed later in Section 5.1) showed that the duration of the impact event between the sand slugs and the Kolsky bar was typically in excess of 0.4 ms. Thus, while the strain gauges could be used to measure the initial force transient exerted by the sand slug, a separate measurement was required in order to estimate the momentum transferred by the sand slug to Kolsky bar.

The measurement of the transmitted momentum was performed by using the Kolsky bar as a ballistic pendulum. Recall that the bar was placed on smooth rollers and thus undergoes rigid body motion due to the momentum transferred by the sand slug. Typically, it is sufficient to approximate the bar as a rigid body after elastic waves due to the impact event have traversed 10 times along the length of the bar, i.e. after 1.8 ms. We measured the steady-state velocity v_{bar} acquired by the bar over a 30 ms duration. Over this time interval, the Kolsky bar can be approximated as a rigid body and thus the transmitted momentum is given as

$$I_t = Mv_{bar} \tag{2.3}$$

where $M = 0.65\,\text{kg}$ is the mass of the Kolsky bar. Note that M is much greater than the mass of the sand slug. Hence v_{bar} is much less than the velocity of the sand slug and it is thus sufficient to regard the Kolsky bar as nominally stationary with respect to the impact of the sand slugs.

3. Overview of the sand launching process

It is instructive to qualitatively describe the phenomena at play during the launch of the sand slugs. The impact of the striker against the piston head imparts a velocity v_o to the piston. Since the mass of the piston is significantly greater than that of the sand slug, v_o remains approximately constant until the piston is abruptly brought to rest by the impact of the piston head against the launcher. The motion of the piston initiates a compressive wave at the interface between the piston and the sand slug. Since the sand slug resides within the cylindrical cavity of the launcher, lateral expansion of the slug is prevented and the sand undergoes uniaxial straining due to this compressive wave. The compressive wave traverses the length of the sand slug and reflects as a tensile wave when it reaches the baking paper covered surface at the distal end from the

piston. (The baking paper is very thin and light and has a negligible effect on wave propagation in the slug, Appendix A.) The sand slug can sustain little or no tension and hence the tensile wave results in spalling of the sand from the free surface. The subsequent deformation of the sand slug is complicated by the interaction of this reflected tensile wave and the compressive waves generated by the continued compression of the rear end of the sand slug by the motion of the piston.

4. Quasi-static characterisation of the dry and wet sand slugs

The compressive response of the sand slugs under uniaxial straining conditions governs the structure of the launched sand slug. Thus, for the sake of completeness we first characterise this response for both the dry and wet sand slugs under quasi-static loading conditions. A cross-sectional view of the set-up used to measure the quasi-static uniaxial straining response of the sand slugs is sketched in Fig. 5a. The set-up comprises a steel block with a cylindrical cavity of diameter 12 mm (equal to that of the sand slug) and a double piston arrangement used to apply the compressive load. Each of the pistons had a rubber O-ring as shown in Fig. 5a that allowed reasonably high pressures to be applied before sand or water squeezed past through the gap between the piston and the cylindrical cavity wall. The dry and wet sand slugs were compacted in the cylindrical cavity exactly in the manner used to prepare the sand slugs as detailed in Section 2.2.

The compressive response of the sand slugs was measured in a screw-driven tests machine. The applied load was measured via the load cell of the test machine while the relative displacement of the pistons was measured via a laser extensometer. The measured applied stress σ versus uniaxial strain ε response of the wet and dry sand slugs is plotted in Fig. 5b. Here, σ is defined as the ratio of the applied force to the cross-sectional area of the cylindrical cavity and ε is the ratio of the measured approach of the two pistons to the initial length $L = 19\,\text{mm}$ of the compressed sand slug. The tests were conducted at an applied strain rate $\dot{\varepsilon} = 10^{-3}\,\text{s}^{-1}$. A series of unloading and re-loading cycles were also conducted in order to gauge the inelastic deformation that occurs during uniaxial compressive loading. The applied stress σ was constrained to <100 MPa as water leaked past the O-ring at higher pressures.

The initial loading response of both the dry and wet sand was linear, albeit the wet sand is nearly 5 times stiffer with $d\sigma / d\varepsilon = 0.98$ GPa for the dry sand while

$d\sigma / d\varepsilon = 4.5$ GPa for the wet sand. Upon unloading, the wet sand nearly re-traced its loading behaviour indicating that the compressive response of the wet sand is essentially linear elastic over the range of stresses investigated here. By contrast, the initial unloading stiffness of the dry sand was 74 GPa with the unloading response becoming strongly non-linear after σ had reduced to less than 20 MPa: this non-linearity gave additional strain recovery. Thus, the compressive response of the dry sand was highly dissipative with significant permanent deformations. For comparison purposes the compressive response of water under uniaxial straining conditions as measured in the same apparatus is included in Fig. 5b. The response was linear elastic with stiffness approximately equal to 2.3 GPa consistent with a wide body of experimental data on the bulk modulus of water [24].

The contrasting responses of the wet and dry sand are rationalised as follows. The sand particles in the fully saturated wet sand slugs are constrained by the water that fills the interstitial spaces between the sand particles. Thus, during compression, the sand particles cannot re-arrange themselves and the response is essentially linear elastic due to the hydrostatic compression of both the water and sand particles. On the other hand, the 40% by volume interstitial spaces between the sand particles in the dry sand slug allows significant re-arrangement of the sand particles to occur during the compression of the slug. The observed inelastic deformation is a consequence of enhanced packing that results from this re-arrangement. We note in passing that for the relatively low applied pressures employed in this study (less than 100 MPa) no fracture of the sand particles was observed: fracture of particles is an additional dissipation mechanism that will be present for higher applied pressures.

5. Dynamic sand slug loading

The observations and measurements made during the dynamic launching of the sand slugs are discussed in this section in two steps. First we characterise the evolution of the sand slug as it is launched and travels towards its target. Then we discuss the measurements made during the impact of the sand slug at the Kolsky bar. At-least two repeat tests were conducted in each case to check the consistency of the measurements. All the results reported in this section had the baking paper front cover on the slugs as described above in Section 3. We show in the Appendix that this cover has a negligible effect on both the deformation of the slug and the pressure exerted by the slug as it impacts the Kolsky bar.

5.1 Characterisation of the evolution of the sand slug

High speed photography was used to observe the sand slug as it exits the launcher and travels towards its target. The high speed photographs were used to characterise the sand slug in terms of the following metrics:

(i) The particle velocity distribution along the length of the slug.
(ii) The total length of the slug.
(iii) The density distribution along the length of the slug.

High speed photographs of the dry and wet sand slugs fired with a piston velocity $v_o = 94\,\mathrm{ms}^{-1}$ are shown in Figure 6. The images pertain to impact against a Kolsky bar at a stand-off $S = 150\,\mathrm{mm}$. Time t indicated in each of the images is measured from the instant of the impact of the striker against the piston head. Here we focus on the images prior to the impact of the sand against the Kolsky bar and discuss the impact process in Section 5.2. As the sand slugs exit the launcher and travel towards the Kolsky bar, the slugs remain approximately cylindrical in cross sectional shape. Moreover, while the diameter of the slugs remains almost unchanged, it is clear that the length of both the wet and dry sand slugs increases with increasing time.

Two key differences are evident between the wet and dry sand slugs. First, the rate of lengthening of the slugs is higher for the dry sand. Second, there is a mushrooming effect at the head of the wet sand slug that is not so prominent in the case of the dry sand slug. This mushrooming effect is due to air resistance effects and is rationalised as follows. The particles of the dry sand move through the air as independent non-interacting particles. Thus, the air only exerts a drag effect on the motion of the particles (it will be shown subsequently that this drag has a negligible effect on the particle velocity) which does not result in the deformation of the slug. By contrast, when water fills in the interstitial spaces between the particles in the wet sand slug, an interaction exists between the sand particles, and the wet sand slug behaves like a continuum material with low shear strength. The pressure on the head of the slug due to the air resistance causes deformation of the column and the mushrooming effect. This is analogous to the deformation of a low shear strength cylindrical projectile after it impacts a rigid target in the Taylor impact test [25]. A similar mushrooming effect has also been observed by Bowden and Brunton [26] for a slug of water moving through air at high velocities.

A similar sequence of high speed video photographs for dry and wet sand slugs fired

with a piston velocity $v_o = 68\,\mathrm{ms}^{-1}$ are shown in Figure 7. The qualitative observations are similar to those detailed above for the $v_o = 94\,\mathrm{ms}^{-1}$ with the main difference being that a smaller mushrooming effect is observed for the wet sand slug which is attributed to the lower air resistance experienced by the slug at this lower velocity.

The high-speed photographs in Figs. 6 and 7 only show the edge of the slug facing the camera. It is unclear from these images if the deformation is planar, i.e. whether plane circular sections across the slug remain planar as the slug deforms. Thus, some additional tests were conducted with a mirror placed at 45° as sketched in Fig. 8a in order to view the part of the slug facing away from the high speed camera. A sequence of images taken for the wet sand slug impacted at $v_o = 68\,\mathrm{ms}^{-1}$ is included in Fig. 8b where both the images of the direct image of the slug and the reflected image are present. Comparing the direct and reflected images, it is clear that the variations across the diameter of the slug are small and that for all practical purposes it is reasonable to assume that plane sections across the slug remain planar with increasing time. This assumption is employed in all the subsequent analyses that quantify the deformation of the slug.

We proceed to analyse the evolution of the slug in terms of the metrics listed above. The particle velocities along the length of the slug are measured by tracking the boundaries between the light and dark layers of the sand slug via the high speed photographs. These boundaries are labelled 1 through 6 with the boundary 1 denoting the head of the sand slug as shown in the inset of Fig. 9a. The measured velocities v_b of the six boundaries of the dry and wet sand slugs fired at $v_o = 94\,\mathrm{ms}^{-1}$ are plotted in Figs. 9a and 9b, respectively as function of time, t. Data for a particular boundary is only available after it exits the cylindrical cavity of the launcher. Hence there is a time lag between the start of the data for the consecutive boundary numbers. It is clear from Figs. 9a and 9b that v_b remains approximately constant after the slug exits the launcher, i.e. air resistance does not have a significant deceleration effect over the time-span in Fig. 9. However, there is spatial gradient in the velocities with the head of the slug (i.e. boundary 1) travelling faster than the rear end of the slug (boundary 6). In order to quantify this gradient we plot in Fig. 10 the temporal average boundary velocities $\overline{v}_b$ (i.e. average of v_b over the time durations plotted in Fig. 9) in Figs. 10a and 10b for the $v_o = 68\,\mathrm{ms}^{-1}$ and $94\,\mathrm{ms}^{-1}$ cases, respectively. In Fig. 10 the variation of $\overline{v}_b$ is plotted as a function of position X in the undeformed configuration of the

slug where $X = 0$ corresponds to the head of the slug and $X = L = 19\,\text{mm}$ corresponds to the distal end of the slug as shown in the inset of Fig. 10a. To a reasonable approximation, $\overline{v}_b$ varies linearly with X in all cases with the gradient $\partial \overline{v}_b / \partial X$ higher for the dry sand slugs compared to the wet sand slugs.

The velocity gradient along the length of the slug results in a lengthening of the slugs with increasing t. The total length ℓ of the dry and wet sand slugs as a function of the distance s travelled by the head of the sand slug is plotted in Figs. 11a and 11b, respectively for both piston velocities considered here. (The definition of s is clarified in the sketch in Fig. 11c.) While ℓ can only be measured after the entire sand slug has exited the launcher barrel we have included in Fig. 11 an extrapolation back to $s = 0$ (where $\ell = L = 19\,\text{mm}$ is the initial length of the sand slug). Consistent with the larger spatial gradients $\partial \overline{v}_b / \partial X$ observed for the dry sand slug (Fig. 10), the length of the dry sand slugs is greater than that of the wet sand slugs for any given value of s; compare Figs. 11a and 11b. Moreover, the rate of lengthening of the dry sand slug (with respect to s) is higher for the lower impact velocity $v_o = 68\,\text{ms}^{-1}$ compared to the $v_o = 94\,\text{ms}^{-1}$ case. On the other hand, $\partial \ell / \partial s$ is reasonably independent of v_o in the wet sand slug case (the differences seen in Fig. 11b are within measurement error margins).

Recall that the spatial gradient of the particle velocities, $\partial \overline{v}_b / \partial X$, is almost linear (Fig. 10). This indicates that the slug is lengthening in approximately a spatially uniform manner and does not develop a density gradient along its length. The current (spatially uniform) density ρ of the slug is then related to its initial density ρ_0 via the relation

$$\rho = \rho_0 \frac{L}{\ell} \qquad (5.1)$$

Given the one-to-one relation between ℓ and ρ, the corresponding current density of the slugs is also included on the right-hand y-axes in Fig. 11.

5.2 Impact of the sand slug against the direct impact Kolsky bar

The measurement of the pressure exerted by the sand slug and the momentum transmitted by the slug into a nominally stationary target are discussed in this section. The nominally stationary target is the instrumented magnesium alloy Kolsky bar placed at a stand-off $S = 50\,\text{mm}$ and 150 mm, as shown in Fig. 2. Also in line with the results presented in Section 5.1, measurements are reported for both the dry and wet

sand slugs fired with piston velocities $v_o = 68\,\text{ms}^{-1}$ and $94\,\text{ms}^{-1}$. Thus, in all there are 8 cases considered in this section.

The pressure p exerted by the sand slugs on the Kolsky bar is defined as

$$p \equiv \frac{4F_s}{\pi D^2} \tag{5.2}$$

where F_s is the force measured via the strain gauged Kolsky bar and $D = 12\,\text{mm}$ is the initial diameter of the sand slug. The measured p versus time t_I histories for all eight cases considered here are plotted in Fig. 12. Here t_I is the time measured from the instant of impact of the sand slug against the Kolsky bar with $p = 0$ for $t_I < 0$. Measurements are only included for $t_I \le 0.3\,\text{ms}$ as the arrival of the reflected wave from the distal end of the Kolsky bar complicates the measurements after this time as explained in Section 2.3.

First consider the dry sand slug cases plotted in Figs. 12a and 12c for $v_o = 68\,\text{ms}^{-1}$ and $94\,\text{ms}^{-1}$, respectively. While the measured pressure histories are reasonably independent of the stand-off S, it is clear on comparing Figs. 12a and 12c that the sand slugs fired with a piston velocity $v_o = 94\,\text{ms}^{-1}$ exert a considerably higher pressure than the $v_o = 68\,\text{ms}^{-1}$ case. We proceed to analyse and discuss these measurements.

The high speed photographs (Figs. 6a and 7a) clearly show that upon impact the sand slugs spread laterally against the face of the Kolsky bar. Momentum conservation then suggests that the sand slug exerts a pressure

$$p \approx \rho v^2 \tag{5.3}$$

where ρ is the density of the impacting sand slug and v the particle velocity. We use Eq. (5.3) to predict the pressure exerted by the sand slug from the independent measurements of ρ and v as follows. Over the duration of the pressure data, the change in the density of the sand slug is small and thus we assume that the density ρ is given by the density of the sand slug at the instant of impact. We denote this density by the symbol ρ_I: it can be read-off from the curves in Figs. 11a and 11b by taking $s = S = 50\,\text{mm}$ or $s = S = 150\,\text{mm}$ as appropriate. Recall that the particle velocities within the slug are approximately time-invariant (Fig. 9) and that these velocities vary approximately linearly along the length of the slug (Fig. 10). We therefore fit a linear relation of the form

$$v = v_H - cX \tag{5.4}$$

to the data in Fig. 10, where v_H is the velocity of the head of the slug and c the

spatial gradient of the velocity. These best fit parameters (v_H, c) obtained from a least-square fit are listed in Table 1 for the four cases, i.e. dry and wet sand with piston velocities $v_o = 68\,\text{ms}^{-1}$ and $94\,\text{ms}^{-1}$. The predicted pressure versus time t_I response for a stand-off S is then given as

$$p = \rho_I \left[v_H - cX \right]^2 \tag{5.5}$$

where X is related to the time t_I via the relation

$$t_I + \frac{S}{v_H} = \frac{S + X}{v}. \tag{5.6}$$

Substituting for v from Eq. (5.3), gives the explicit relation between X and t_I as

$$X = \frac{v_H t_I}{1 + ct_I + cS / v_H}. \tag{5.7}$$

Predictions based on Eqs. (5.5) and (5.7) are included in Fig. 13 for the four dry sand slug cases. The values of ρ_I, as read-off from Fig. 11a, and used in these predictions are listed in Table 2.

The measured and predicted pressures are in reasonable agreement for $t_I > 0.05\,\text{ms}$ indicating that the inertial relation, Eq. (5.3) is applicable for the majority of the impact duration. However, there is an initial transient in the measurements that gives pressures significantly greater than ρv^2. Such an initial transient was also reported in the discrete element calculations of the impact of a sand slug by Pingle et al.[18]; these authors attributed this transient to elastic wave propagation effects within the sand slug that are important prior to the steady-state lateral spreading deformation mode being established.

Next consider the wet sand slugs pressure histories plotted in Figs. 12b and 12d for the $v_o = 68\,\text{ms}^{-1}$ and $94\,\text{ms}^{-1}$ cases, respectively. Three key differences are observed when compared with the dry sand pressure histories in Figs. 12a and 12c:

(i) The pressures are higher for the wet sand slug when compared with the corresponding dry sand slug impacts. This difference is primarily due to the fact that the wet sand slug density is higher than the dry sand slug.

(ii) While the peak pressure is independent of stand-off for the dry sand slug, the peak pressures for the wet sand slug at $S = 150\,\text{mm}$ are significantly lower compared to the corresponding peak pressure at $S = 50\,\text{mm}$. We attribute this reduction to the mushrooming seen at the head of the wet sand slug that increases with increasing distance travelled by the sand slug. The dry sand slug does not display this mushrooming effect and hence the peak

pressures are independent of stand-off.

(iii) Large oscillations are observed in the measured pressure versus time history of the wet sand slug immediately after the peak pressure. These oscillations are not observed during the impact of dry sand slugs. While the precise source of these oscillations is unclear, they might be related to the Plateau-Rayleigh instability [27] which results in the sand/water mixture breaking-up into smaller packets - the discrete impact of these packets might give rise to the observed oscillations. By contrast, the dry sand slug comprises independent sand particles and hence a similar instability cannot occur in this case.

Comparisons between the measured pressure histories and predictions based on Eqs. (5.5) and (5.7) showed similar trends to the dry sand slug case (Fig. 13), i.e. the predictions captured the tail of the pressure history accurately but did not predict the initial peak pressures. Hence, we omit these comparisons for the sake of brevity.

We now proceed to quantify the momentum transferred to the stationary target by the sand slugs. The incoming momentum of the sand slug is calculated as

$$I_o = \frac{\pi D^2}{4} \rho_o \int_0^L v dX \qquad (5.8)$$

where v is given by Eq. (5.4). The momentum transmitted I_t into the target is determined by measuring the velocity that the Kolsky bar acquires as detailed in Section 2.3. The ratio I_t / I_o is a measure of the so-called fluid-structure interaction effect. If the sand upon impacting the target flows laterally with no bounce-back, then $I_t / I_o = 1$; while $I_t / I_o > 1$ corresponds to the case where some fraction of the sand rebounds off the target. The measured values of I_o, I_t and I_t / I_o are listed in Table 3 for the eight cases considered here. In all cases $I_t / I_o \approx 1$: any deviations from $I_t / I_o = 1$ seen in Table 3 are within the error margins associated with the measurements made in this study.

There is a significant literature suggesting that the impact of wet sand on structures is far more destructive compared to equivalent dry sand impacts. There two potential reasons for this:

(i) The fluid-structure interaction between wet sand and structures is such that $I_t / I_o > 1$ for wet sand impacts while $I_t / I_o \approx 1$ for dry sand impacts, or

(ii) Wet sand has a higher density compared to dry sand. Thus, for the same

impact velocity the wet sand has a higher momentum and hence transmits more impulse into the structure compared to dry sand.
The results presented here are consistent with (ii), i.e. $I_t / I_o \approx 1$ for both wet and dry sand impacts with I_t of the wet sand being higher due to the extra mass of water.

Pingle et al. [18] modelled slugs comprising discrete particles that impact rigid-stationary structures. The numerical results showed that the pressure exerted by the slugs is well approximated as $p = \rho v^2$, where ρ is the effective density of the slug and v the velocity of the impacting particles. Moreover, the momentum I_t transferred to the structure from the sand slug is approximately equal to the free-field incoming momentum of the sand slug. The experimental results presented here are in agreement with these numerical results and thus confirm that the loading of structures due to the sand is primarily inertial. While Pingle et al. [18] only modelled dry sand, the experimental results here indicate that the main conclusions of that study carry forward to wet sand as well.

6. Concluding remarks

A laboratory-based methodology to launch cylindrical sand slugs at high velocities has been developed. Both dry and fully water saturated sand slugs (wet sand slugs) were launched, and the time evolution of these slugs has been characterised. The sand slugs are initially at rest within a cylindrical barrel and were launched by the impact of a piston at the rear end of the stationary slug. This impact process results in the slugs having an approximately linear axial gradient of particle velocities with the sand particles at the head of the slug having a higher velocity compared to those at the rear. This means that the slugs lengthen as they travel towards their target. However, the sand particles acquire nearly no radial velocity, and hence the diameter of the slugs remains unchanged with increasing time. The linear spatial gradient in the velocity means that while the density of the slugs decrease with increasing time, the slugs remain spatially homogenous with no associated density gradient. In general the dry sand slugs have a higher velocity gradient compared to the wet sand slugs.

The pressure exerted by the sand slugs on a rigid and nominally stationary target was measured by impacting the slugs against an instrumented direct impact Kolsky bar. After an initial high transient pressure, the pressure reduced to a value equal to approximately ρv^2 where ρ is the density of the impacting sand slug and v the particle velocity. This measured pressure is consistent with the observation that the

impacted sand flows laterally on the face of the Kolsky bar and clearly shows that the loading due to the sand is primarily inertial. The wet sand slugs typically exert a higher pressure due to their higher densities. The ratio of the transmitted to incident momentum was approximately unity in all cases as there was negligible rebound of the impacting sand slugs. This indicates that there are no differences in the so-called fluid-structure interaction effects between wet and dry sand slugs.

This experimental study has clearly highlighted some key differences between wet and dry sand aggregates travelling at high velocities. This includes the fact that dry sand slugs lengthen at a faster rate compared to wet sand slugs and that wet sand slugs display a mushrooming effect at the head of the slug. Numerical simulations are required to understand these differences. This is a topic for future research.

Appendix: Effect of the baking paper front cover

A baking paper front cover was used to help maintain the shape of the sand slug within the launcher cavity. While this cover is essential for dry sand, the higher cohesive strength of the water saturated sand allows the wet sand slug to maintain its shape without the front cover. We thus repeated some of the wet sand experiments without the baking paper front cover in order to gauge the influence of this cover on the measurements reported in the main part of this study.

A comparison between the measured pressure p versus time t_1 histories for the wet sand slugs launched with a piston velocity $v_o = 68\,\mathrm{ms}^{-1}$ with and without the baking paper front cover is shown in Figs. A1a and A1b for stand-off values $S = 50\,\mathrm{mm}$ and 150 mm, respectively. To within the scatter associated with these measurements, the results with and without the front cover are indistinguishable. A sequence of high speed photographs of the wet sand slug without the front cover launched with $v_o = 68\,\mathrm{ms}^{-1}$ is included in Fig. A1c. These images confirm that the evolution of the slug is also unaffected by the presence of front cover; compare Fig. 7b and Fig. A1c. We thus conclude that the front cover has a negligible effect on both the deformation of the slug and the pressure exerted by the sand slugs on the target.

Acknowledgements

The authors are grateful to Vernon Joynt and Keith Williams of General Dynamics for providing the high speed video images of a buried explosive event and for many helpful discussions. The research was supported by the Office of Naval Research under ONR contract N00014-09-1-0573 (Dr D. Shifler, Programme Manager).

References

[1] H.N.G. Wadley, K.P. Dharmasena, D.T. Queheillalt, Y. Chen, P. Dudt, D. Knight, K. Kiddy, Z. Xue, A. Vaziri. *Dynamic compression of square honeycomb structures subjected to impulsive underwater loading*. J. Mech. Mat. Struc. 10 (2007) 2025–2048.

[2] H.D. Espinosa, S. Lee, N. Moldova. *A novel fluid structure interaction experiment to investigate deformation of structural elements subjected to impulsive loading*. Exp. Mech. 46 (2006) 805–824.

[3] V.S. Deshpande, A. Heaver, N.A. Fleck. *An underwater shock simulator*. Proc. R. Soc. A, 462 (2006) 1021–1041.

[4] N. Kambouchev, L. Noels, R. Radovitzky. *Nonlinear compressibility effects in fluid-structure interaction and their implications on the air-blast loading of structures*. J. Appl. Phys. 100 (2006).

[5] A. Vaziri, J.W. Hutchinson. *Metal sandwich plates subject to intense air shocks*. Int. J. Solids Struc. 44 (2007) 2021–2035.

[6] H.N.G. Wadley, K.P. Dharmasena, M.Y. He, R.M. McMeeking, A.G. Evans, T. Bui-Thanh, R. Radovitzky. *An active concept for limiting injuries caused by air blast*s. Int. J. Impact Eng. 37 (2010) 317-323.

[7] A. Neuberger, S. Peles, D. Rittel, *Scaling the response of circular plates subjected to large and close-range spherical explosions. Part I: Air-blast loading*, International Journal of Impact Engineering 34 (2007) 859–873.

[8] P.S. Westine, B.L. Morris, P.A. Cox, P.A., E. Polch, *Development of computer*

program for floor plate response from land mine explosions. Contract Report No. 1345 for US Army TACOM Research and Development Centre, (1985).

[9] A. Neuberger, S. Peles, D. Rittel, *Scaling the response of circular plates subjected to large and close-range spherical explosions. Part II: Buried charges*, International Journal of Impact Engineering 34 (2007) 874–882.

[10] B.L. Morris. *Analysis of improved crew survivability in light vehicles subjected to mine blast*. Final report for Contract No. DAAK70-92-C-0058 for the US Army Belvoir RDEC, Ft. Belvoir, VA; 1993.

[11] J.J. Rimoli, B. Talamini, J.J. Wetzel, K.P. Dharmasena, R. Radovitzky and H.N.G. Wadley, Wet-Sand Impulse Loading of Metallic Plates and Corrugated Core Sandwich Panels, *International Journal of Impact Engineering* , 38, (2011), 837-848.

[12] V.S. Deshpande, R.M. McMeeking, H.N.G. Wadley and A.G. Evans, "Constitutive Model for Predicting Dynamic Interactions Between Soil Ejecta and Structural Panels ", Journal of Mechanics and Physics of Solids , 57, (2009) 1139-1164.

[13] M. Grujicic, B. Pandurangan, R. Qiao, B.A. Cheeseman, W.N. Roy, R.R. Skaggs, R. Gupta. *Parameterization of the porous-material model for sand with different levels of water saturation*. Soil dyn. Earthq. Eng. 28 (2008) 20–35.

[14] Z. Wang, H. Hao, Y. Lu. *A three-phase soil model for simulating stress wave propagation due to blast loading*. Int. J. Numer. Anal. Methods Geomech. 28 (2004) 33–56.

[15] D. Bergeron, J.E. Tremblay. *Canadian research to characterize mine blast output*. In: Proceedings of the 16th International MABS Symposium, Oxford, UK, 2000.

[16] J. Foedinger. *Methodology for improved characterization of landmine explosions, SBIR Phase-II plus program*. In: Proceedings of the Technical Interchange Meeting, Material Science Corporation, 2005.

[17] T. Børvik, L. Olovsson, A.G. Hanssen, K.P. Dharmasena, H. Hansson, H.N.G.

Wadley. *A discrete particle approach to simulate the combined effect of blast and sand impact loading of steel plates*. J. Mech. Phys. Solids 59 (2011) 940-958.

[18] S.M. Pingle, N.A. Fleck, H.N.G. Wadley, V.S. Deshpande, *Discrete element calculations of the impact of a sand column against rigid structures*, (2011), submitted.

[19] G.I. Taylor. The pressure and impulse of submarine explosion waves on plates. In The scientific papers of G I Taylor, vol. III, pp. 287–303. Cambridge: Cambridge University Press, 1963.

[20] T. Liu, N.A. Fleck, V.S. Deshpande, H.N.G. Wadley. *The impact of sand slugs against beams and plates: coupled discrete/continuum calculations*, (2011), submitted.

[21] V. Joynt, K, Williams, Private communication, 2010.

[22] O.A. Shergold, N.A. Fleck, D.D. Radford. *The uniaxial stress versus strain response of pig skin and silicone rubber at low and high strain rate*. Int. J. Impact Eng. 32 (2006) 1384–1402.

[23] V.L. Tagarielli, V.S. Deshpande, N.A. Fleck. *The high strain rate response of PVC foams and end-grain balsa wood*. Comp.: Part B 39 (2008) 83–91.

[24] W.P. Graebel. *Engineering fluid mechanics*. Taylor & Francis, New York, 2001.

[25] G.I. Taylor. *The use of flat ended projectiles for determining yield stress. I. Theoretical considerations.* Proc. R. Soc. London. A. (1948), 194, 289–299.

[26] F.P. Bowden, J.H. Brunton. *The Deformation of Solids by Liquid Impact at Supersonic Speeds*. Proc. R. Soc. London. A, Math. and Phys. 263 (1961) 433-450.

[27] L. Rayleigh. *On the instability of jets*. Proc. London Math. Soc. s1-10 (1878) 4-13.

List of figures

Fig 1: (a) Sketch of the sand/structure interaction problem analysed by Liu et al. [20] where a cylindrical slug of sand particles impacts a clamped plate. (b) High speed photographs showing the soil ejecta resulting from the detonation of a landmine buried under water saturated soil. The inter-frame time is 0.182ms. Images adapted from Joynt and Williams [21].

Fig. 2: Sketch of the apparatus used to launch the sand slugs. The instrumented direct impact Kolsky bar at a stand-off S is also included in the figure. The sketch is labelled with all leading dimensions in mm.

Fig. 3: Optical micrographs of the sand particles used in both the dry and wet sand slugs.

Fig. 4: Sketch of the circuit used for measuring strain in the Kolsky bar by recording the change in voltage across a fixed resistor.

Fig. 5: (a) Sketch of the apparatus used to measure the quasi-static compressive response of the dry and wet sand slugs. (b) The measured applied axial stress σ versus uniaxial strain ε responses of the wet and dry sand slugs. The corresponding uniaxial compressive response of water is also included.

Fig. 6: High speed photographs the (a) dry and (b) wet sand slugs launched with a piston velocity $v_o = 94\,\mathrm{ms}^{-1}$. The slugs impact the Kolsky bar placed at a stand-off $S = 150\,\mathrm{mm}$. The time t for each image is also included with time $t = 0$ corresponding to the instant that the striker impacts the piston.

Fig. 7: High speed photographs the (a) dry and (b) wet sand slugs launched with a piston velocity $v_o = 68\,\mathrm{ms}^{-1}$. The slugs impact the Kolsky bar placed at a stand-off $S = 150\,\mathrm{mm}$. The time t for each image is also included with time $t = 0$ corresponding to the instant that the striker impacts the piston.

Fig. 8: (a) Sketch of a mirror arrangement used to visualise the edge of the sand slug facing away from the high speed camera. (b) High speed images showing both the

direct and reflected images of the wet sand slug launched with a piston velocity $v_o = 68\,\mathrm{ms}^{-1}$. The slugs impact the Kolsky bar placed at a stand-off $S = 150\,\mathrm{mm}$. The time t for each image is also included with time $t = 0$ corresponding to the instant that the striker impacts the piston.

Fig 9: The measured boundary velocities v_b as a function of time t for the (a) dry and (b) wet sand slugs launched with a piston velocity $v_o = 94\,\mathrm{ms}^{-1}$. Time $t = 0$ corresponds to the instant that the striker impacts the piston. The boundary labelling is shown on a sketch of the "zebra striped" sand slug which is included as an inset in (a).

Fig. 10: The temporal average velocities $\overline{v}_b$ of the boundaries 1 through 6 for slugs launched with a piston velocity (a) $v_o = 68\,\mathrm{ms}^{-1}$ and (b) $v_o = 94\,\mathrm{ms}^{-1}$. The velocities $\overline{v}_b$ are plotted as a function of their spatial position X in the un-deformed configuration. The co-ordinate X is defined in the inset in (a).

Fig. 11: The evolution of the length ℓ of the (a) dry and (b) wet slugs as a function of the distance s travelled by the head of the slug. The figures have a dual y-axis with the corresponding density ρ of the sand slugs labelled on the right-hand y-axis. (c) Sketch illustrating the definition of s.

Fig. 12: The measured pressure p versus time t_I histories for the impact of the dry sand slugs launched with a piston velocity (a) $v_o = 68\,\mathrm{ms}^{-1}$ and (c) $v_o = 94\,\mathrm{ms}^{-1}$. The corresponding measurements for the wet sand slugs are plotted in (b) for $v_o = 68\,\mathrm{ms}^{-1}$ and (d) for $v_o = 94\,\mathrm{ms}^{-1}$. In each case results are shown for stand-offs $S = 50\,\mathrm{mm}$ and 150 mm. Here time $t_I = 0$ is defined as the instant the slug impacts the Kolsky bar.

Fig. 13: Comparison between the measured and predicted pressure versus time t_I histories for the impact of the dry sand slug. Results are shown for both values of the

piston velocities v_o and stand-offs S considered in this study. (a) $v_o = 68\,\text{ms}^{-1}$ and $S = 50\,\text{mm}$, (b) $v_o = 68\,\text{ms}^{-1}$ and $S = 150\,\text{mm}$, (c) $v_o = 94\,\text{ms}^{-1}$ and $S = 50\,\text{mm}$ and (d) $v_o = 94\,\text{ms}^{-1}$ and $S = 150\,\text{mm}$.

Fig. A1: Comparison between the measured pressure versus time t_1 histories for the wet sand slug with and without the baking paper front cover. Results are shown for slugs launched with a piston velocity $v_o = 68\,\text{ms}^{-1}$ and a stand-off (a) $S = 50\,\text{mm}$ and (b) $S = 150\,\text{mm}$. (c) A montage of high-speed photographs of the wet sand slug without the baking paper front cover launched with $v_o = 68\,\text{ms}^{-1}$ and impacting the Kolsky bar at a stand-off $S = 150\,\text{mm}$. The time t for each image is also included with time $t = 0$ corresponding to the instant that the striker impacts the piston.

List of Tables:

Table 1: The values of parameters (v_H, c) obtained by performing a least-square fit of Eq. (5.4) to the data in Fig. 10.

Table 2: The density ρ_1 of the sand slugs just prior to the impact against the Kolsky bar. These values are read-off from Fig. 11 and used in the pressure predictions in Fig. 13.

Table 3: The measured sand slug impulses for all 8 cases considered in this study. The table lists the incident or free-field impulses I_o, the impulse I_t transmitted into the Kolsky bar and the ratio I_t / I_o.

Tables

Saturation-state	v_0 (ms^{-1})	v_H (ms^{-1})	c (s^{-1})
Dry	68	92	1845
	94	127	2080
Wet	68	82	730
	94	119	1370

Table 1: The values of parameters (v_H, c) obtained by performing a least-square fit of Eq. (5.4) to the data in Fig. 10.

v_0 (ms^{-1})	S (mm)	ρ_I (kgm^{-3})
68	50	820
	150	429
94	50	1069
	150	530

Table 2: The density ρ_I of the sand slugs just prior to the impact against the Kolsky bar. These values are read-off from Fig. 11 and used in the pressure predictions in Fig. 13.

Stand off, S (mm)	Saturation-state	Piston velocity v_o (ms^{-1})	Incident momentum I_o (Ns)	Transmitted momentum I_t (Ns)	I_t / I_o
150	Dry	68	0.264	0.267	1.01
		94	0.380	0.384	1.01
50	Dry	68	0.264	0.268	1.01
		94	0.264	0.384	1.02
150	Wet	68	0.323	0.324	1.00
		94	0.455	0.456	1.00
50	Wet	68	0.323	0.319	0.99
		94	0.455	0.464	1.02

Table 3: The measured sand slug impulses for all 8 cases considered in this study. The table lists the incident or free-field impulses I_o, the impulse I_t transmitted into the Kolsky bar and the ratio I_t / I_o.

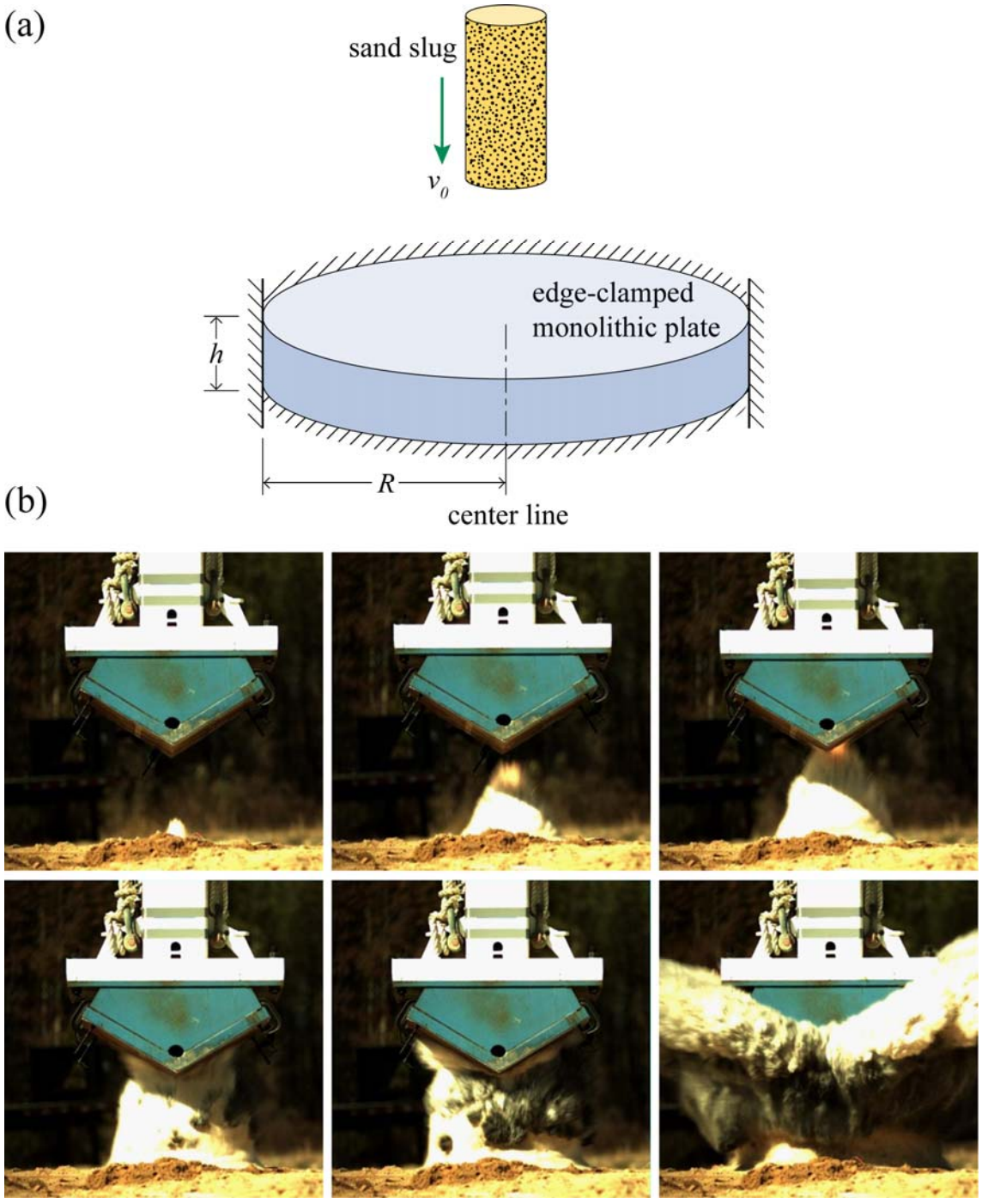

Fig 1: (a) Sketch of the sand/structure interaction problem analysed by Liu et al. [20] where a cylindrical slug of sand particles impacts a clamped plate. (b) High speed photographs showing the soil ejecta resulting from the detonation of a landmine buried under water saturated soil. The inter-frame time is 0.182ms. Images adapted from Joynt and Williams [21].

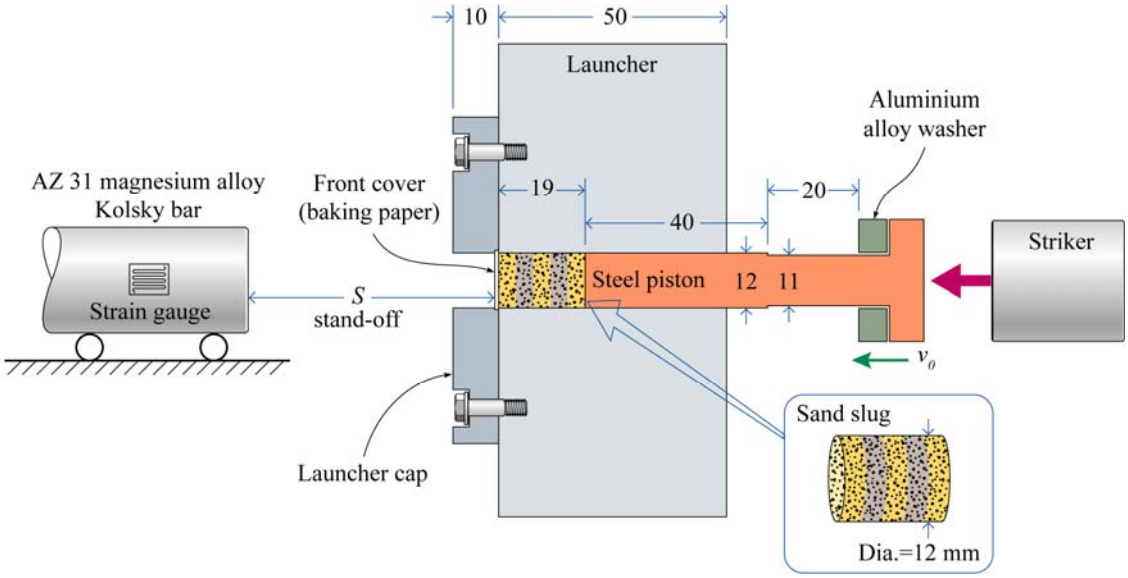

Fig. 2: Sketch of the apparatus used to launch the sand slugs. The instrumented direct impact Kolsky bar at a stand-off S is also included in the figure. The sketch is labelled with all leading dimensions in mm.

Fig. 3: Optical micrographs of the sand particles used in both the dry and wet sand slugs.

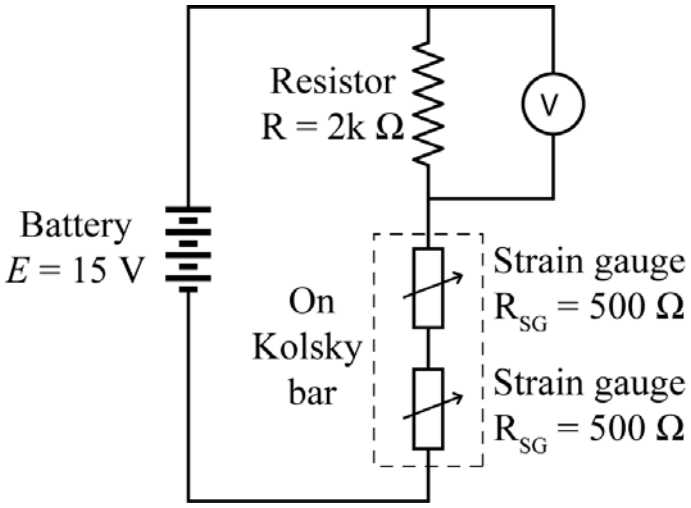

Fig. 4: Sketch of the circuit used for measuring strain in the Kolsky bar by recording the change in voltage across a fixed resistor.

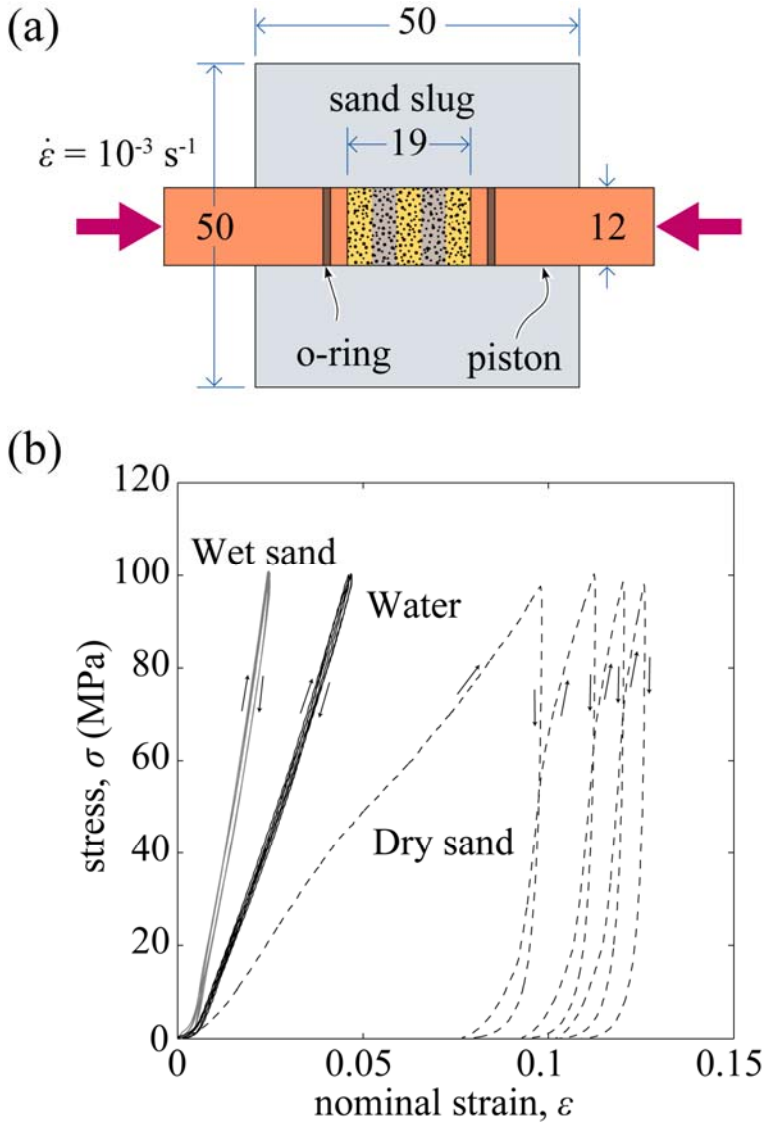

Fig. 5: (a) Sketch of the apparatus used to measure the quasi-static compressive response of the dry and wet sand slugs. All dimensions are in mm. (b) The measured applied axial stress σ versus uniaxial strain ε responses of the wet and dry sand slugs. The corresponding uniaxial compressive response of water is also included.

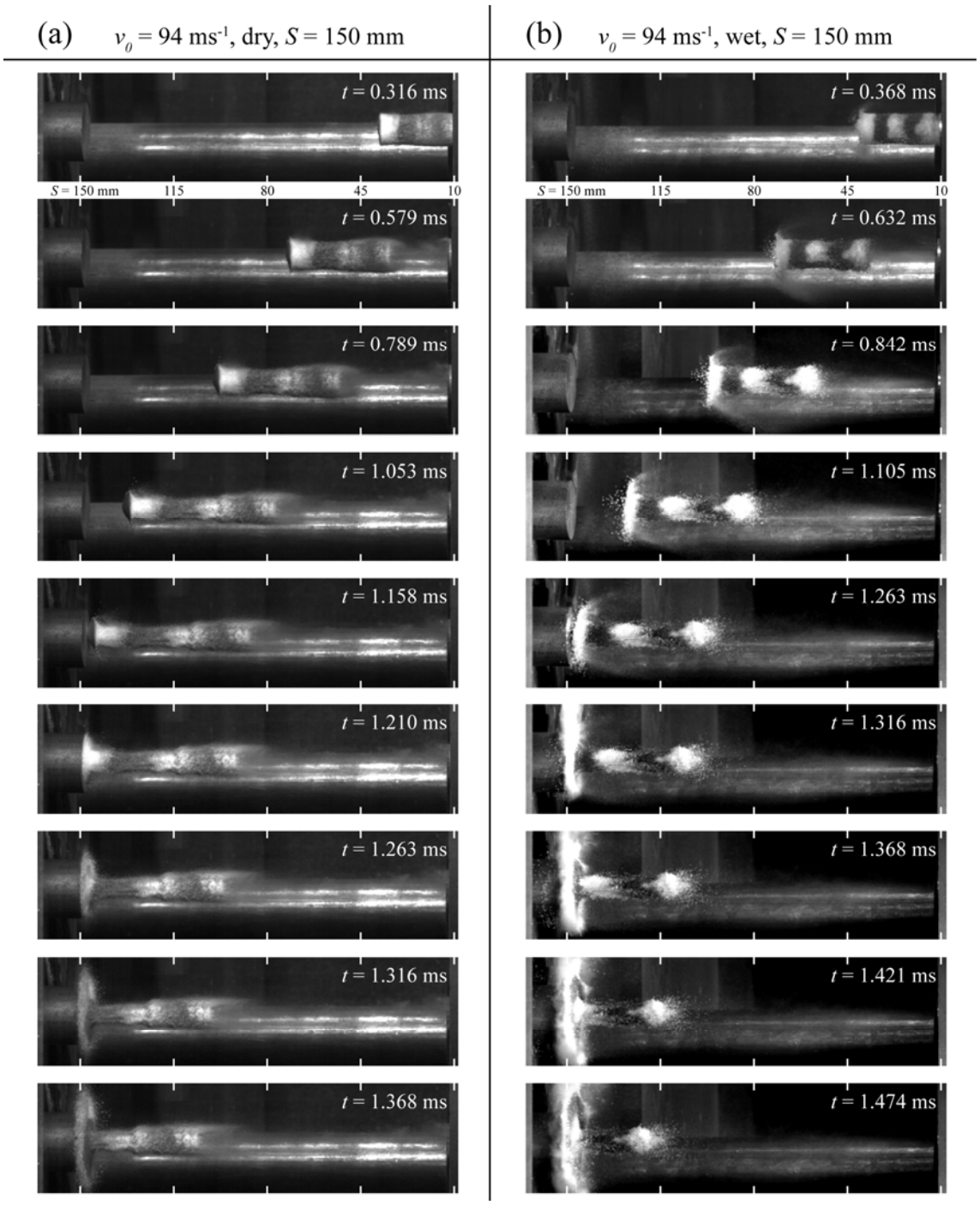

Fig. 6: High speed photographs the (a) dry and (b) wet sand slugs launched with a piston velocity $v_o = 94\,\text{ms}^{-1}$. The slugs impact the Kolsky bar placed at a stand-off $S = 150\,\text{mm}$. The time t for each image is also included with time $t = 0$ corresponding to the instant that the striker impacts the piston.

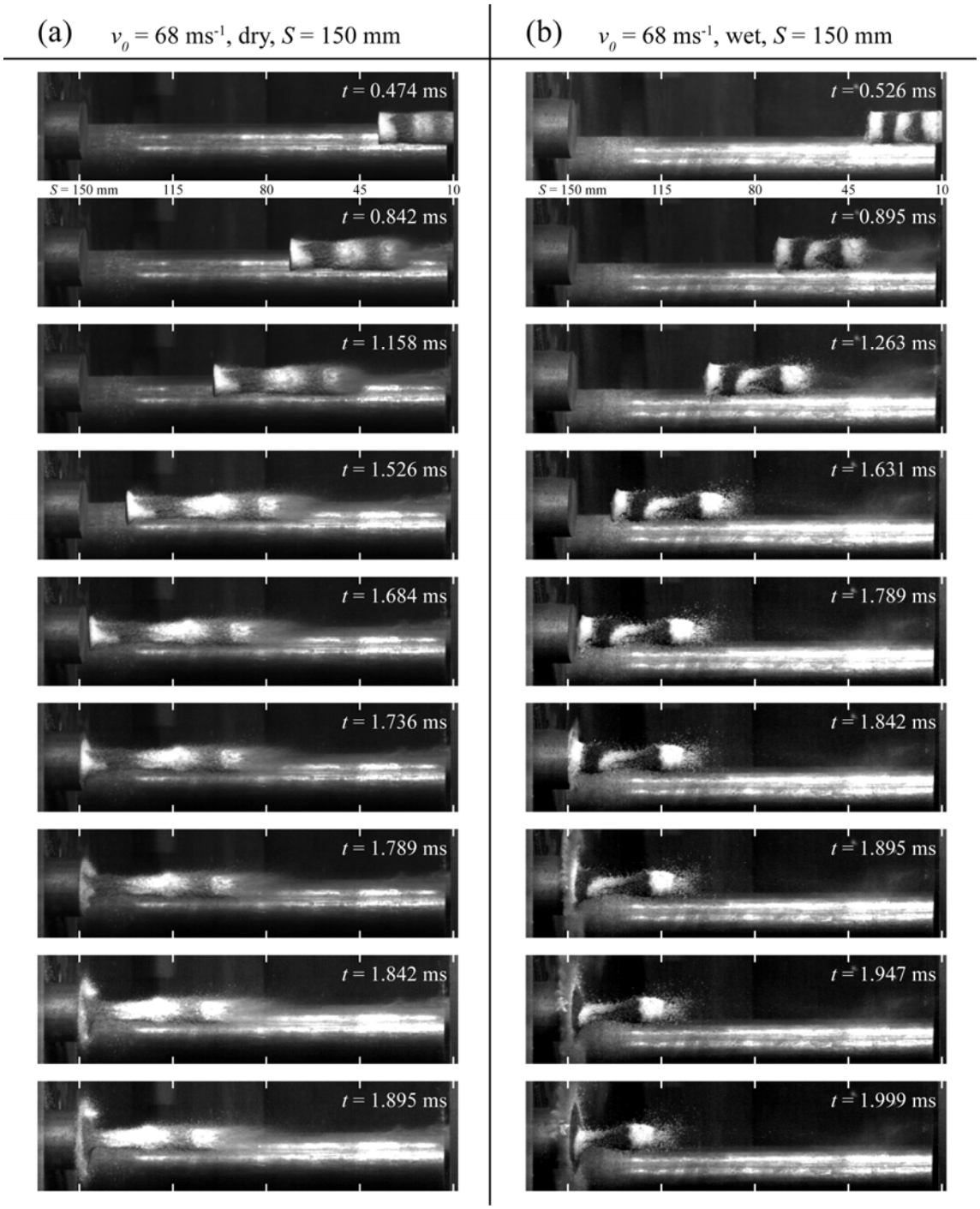

Fig. 7: High speed photographs the (a) dry and (b) wet sand slugs launched with a piston velocity $v_o = 68\,\mathrm{ms}^{-1}$. The slugs impact the Kolsky bar placed at a stand-off $S = 150\,\mathrm{mm}$. The time t for each image is also included with time $t = 0$ corresponding to the instant that the striker impacts the piston.

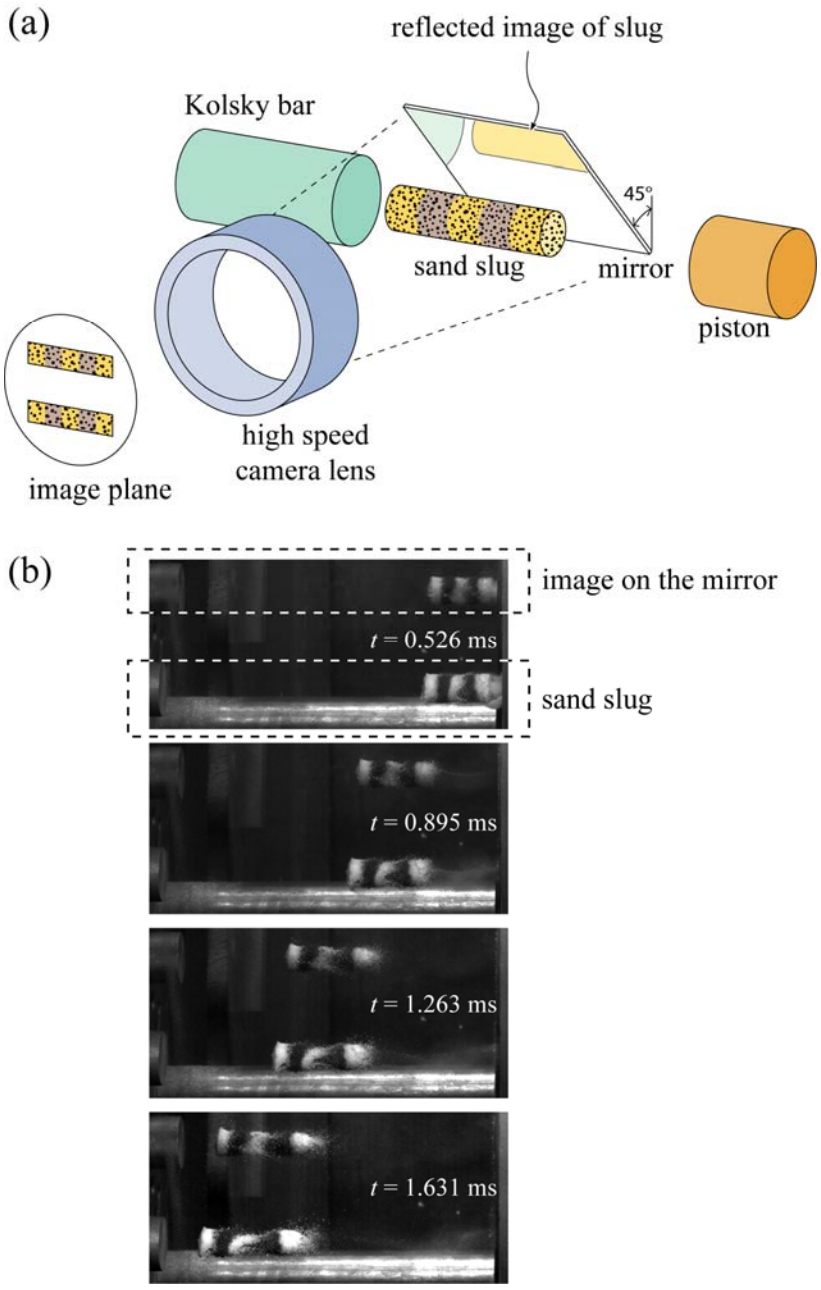

Fig. 8: (a) Sketch of a mirror arrangement used to visualise the edge of the sand slug facing away from the high speed camera. (b) High speed images showing both the direct and reflected images of the wet sand slug launched with a piston velocity $v_o = 68\,\mathrm{ms}^{-1}$. The slugs impact the Kolsky bar placed at a stand-off $S = 150\,\mathrm{mm}$. The time t for each image is also included with time $t = 0$ corresponding to the instant that the striker impacts the piston.

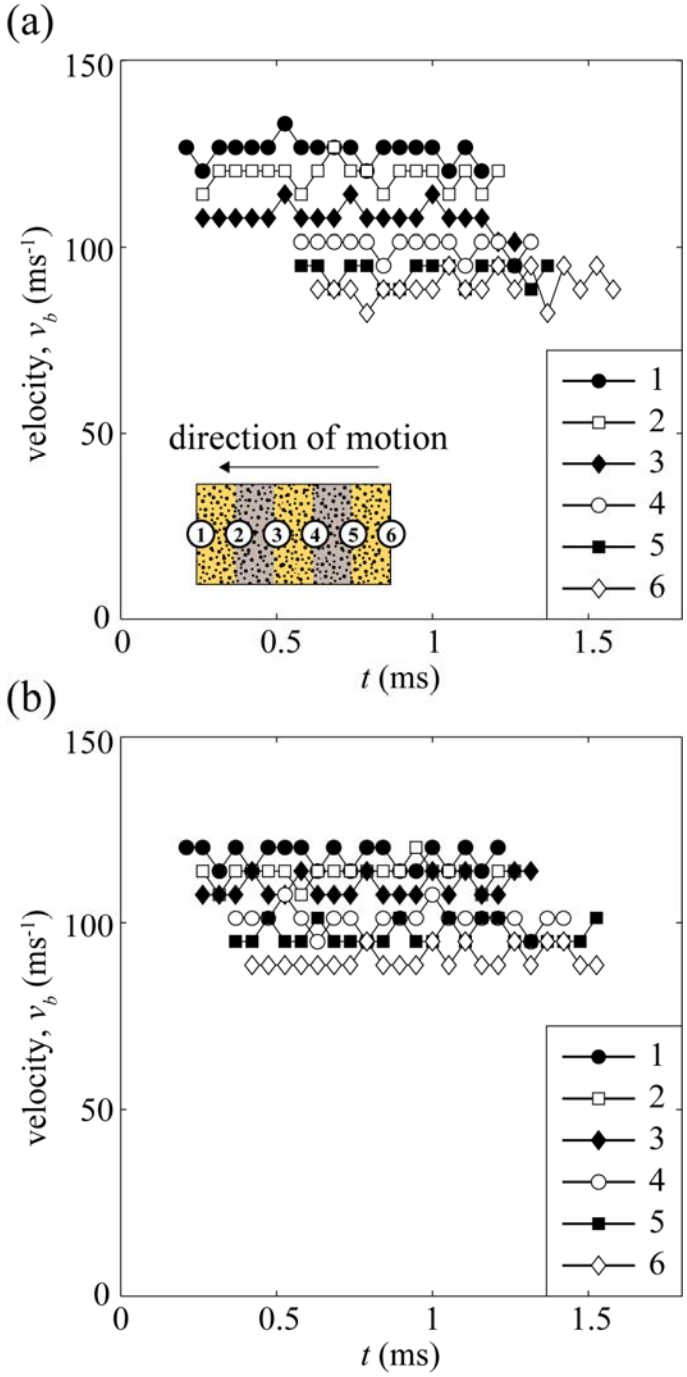

Fig 9: The measured boundary velocities v_b as a function of time t for the (a) dry and (b) wet sand slugs launched with a piston velocity $v_o = 94\,\text{ms}^{-1}$. Time $t = 0$ corresponds to the instant that the striker impacts the piston. The boundary labelling is shown on a sketch of the "zebra striped" sand slug which is included as an inset in (a).

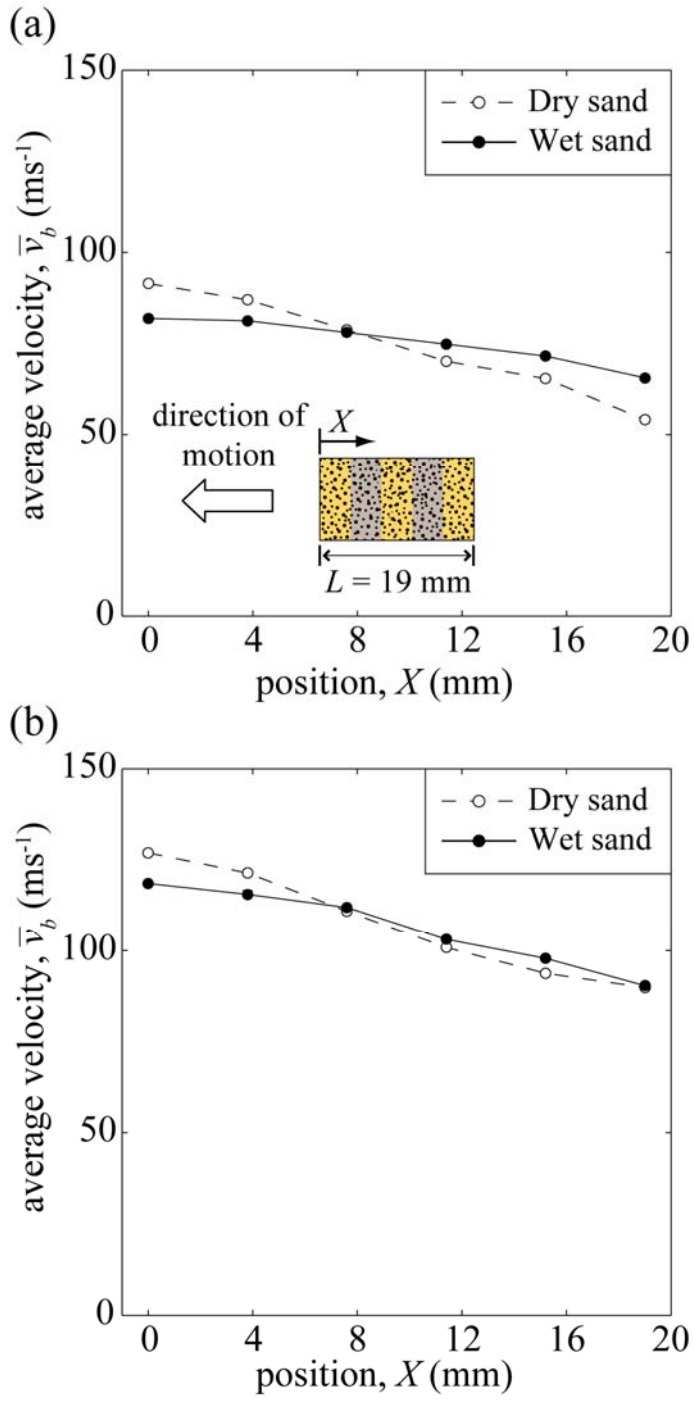

Fig. 10: The temporal average velocities $\overline{v}_b$ of the boundaries 1 through 6 for slugs launched with a piston velocity (a) $v_o = 68\,\text{ms}^{-1}$ and (b) $v_o = 94\,\text{ms}^{-1}$. The velocities $\overline{v}_b$ are plotted as a function of their spatial position X in the un-deformed configuration. The co-ordinate X is defined in the inset in (a).

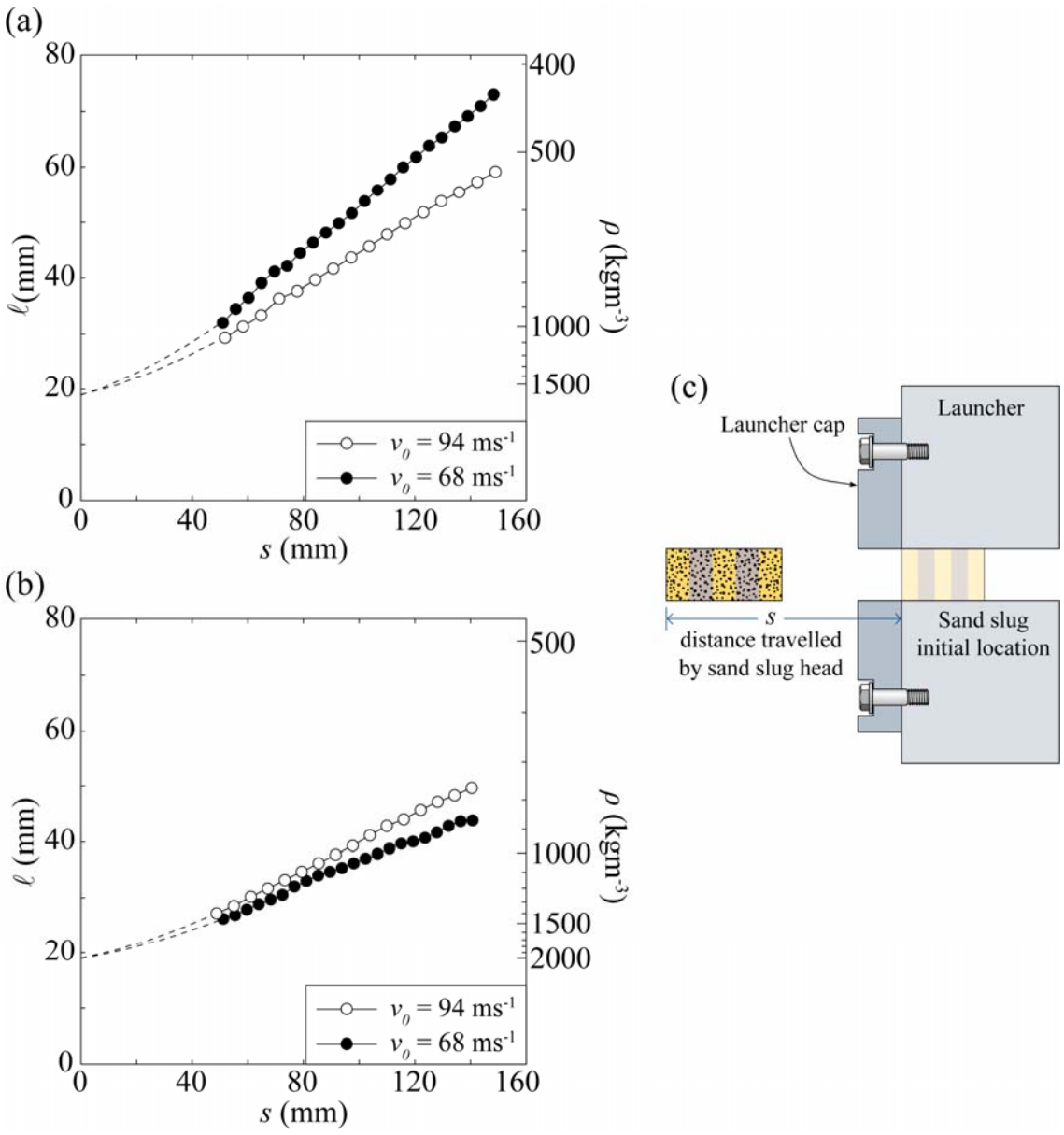

Fig. 11: The evolution of the length ℓ of the (a) dry and (b) wet sand slugs as a function of the distance s travelled by the head of the slug. The figures have a dual y-axis with the corresponding density ρ of the sand slugs labelled on the right-hand y-axis. (c) Sketch illustrating the definition of s.

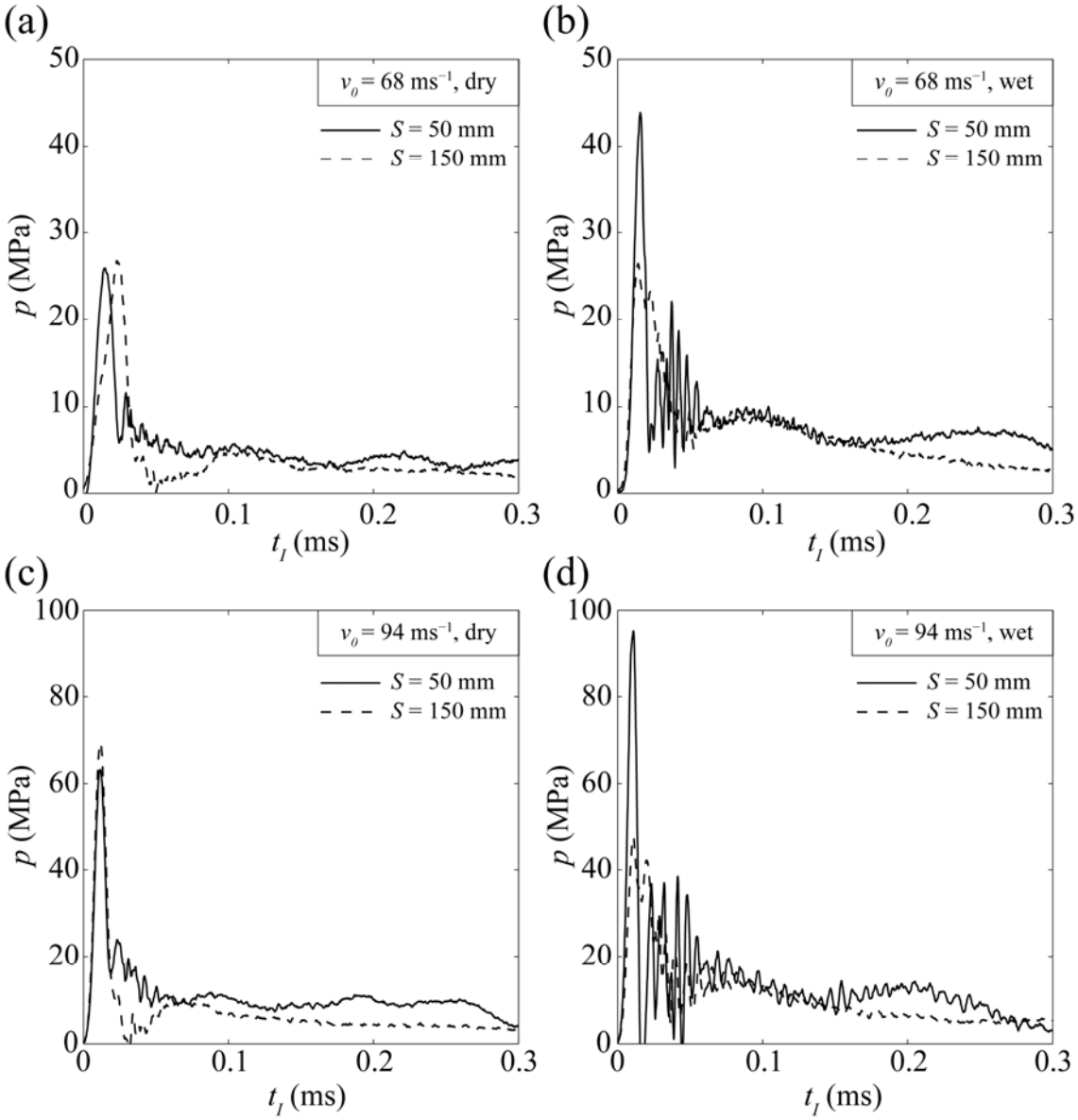

Fig. 12: The measured pressure p versus time t_1 histories for the impact of the dry sand slugs launched with a piston velocity (a) $v_o = 68\,\text{ms}^{-1}$ and (c) $v_o = 94\,\text{ms}^{-1}$. The corresponding measurements for the wet sand slugs are plotted in (b) for $v_o = 68\,\text{ms}^{-1}$ and (d) for $v_o = 94\,\text{ms}^{-1}$. In each case results are shown for stand-offs $S = 50\,\text{mm}$ and 150 mm. Here time $t_1 = 0$ is defined as the instant the slug impacts the Kolsky bar.

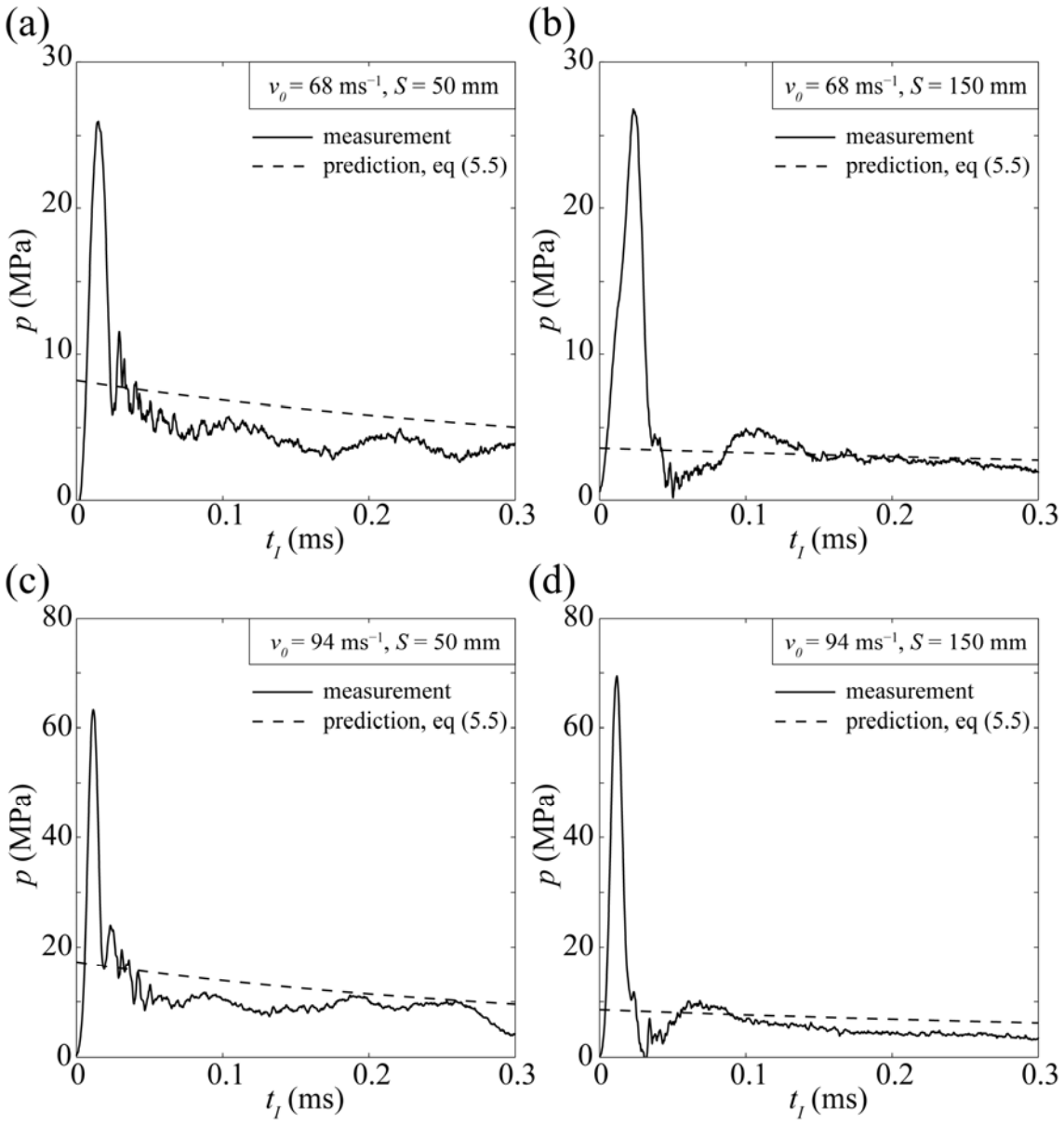

Fig. 13: Comparison between the measured and predicted pressure versus time t_I histories for the impact of the dry sand slug. Results are shown for both values of the piston velocities v_o and stand-offs S considered in this study. (a) $v_o = 68\,\text{ms}^{-1}$ and $S = 50\,\text{mm}$, (b) $v_o = 68\,\text{ms}^{-1}$ and $S = 150\,\text{mm}$, (c) $v_o = 94\,\text{ms}^{-1}$ and $S = 50\,\text{mm}$ and (d) $v_o = 94\,\text{ms}^{-1}$ and $S = 150\,\text{mm}$.

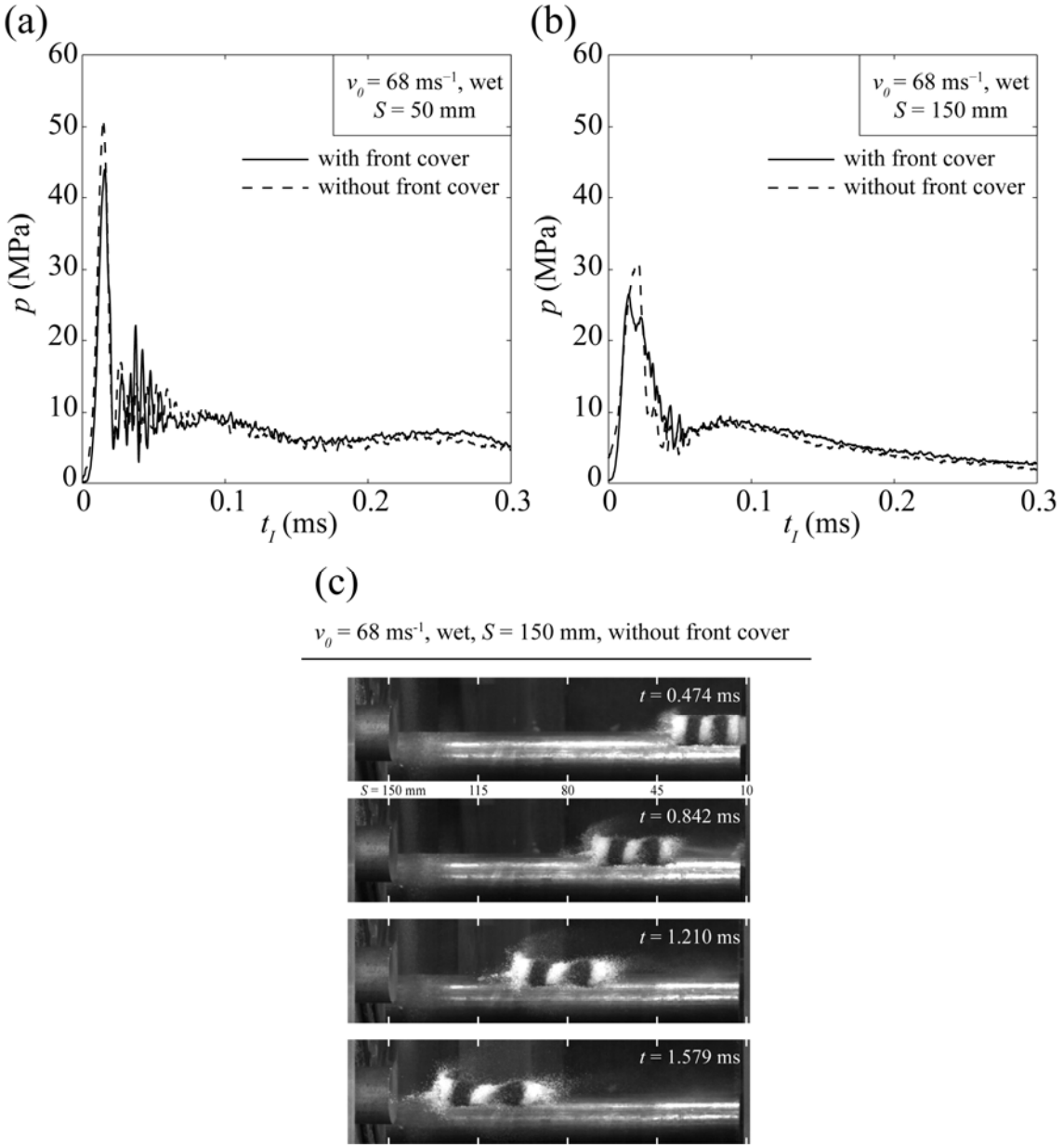

Fig. A1: Comparison between the measured pressure versus time t_1 histories for the wet sand slug with and without the baking paper front cover. Results are shown for slugs launched with a piston velocity $v_o = 68\,\text{ms}^{-1}$ and a stand-off (a) $S = 50\,\text{mm}$ and (b) $S = 150\,\text{mm}$. (c) A montage of high-speed photographs of the wet sand slug without the baking paper front cover launched with $v_o = 68\,\text{ms}^{-1}$ and impacting the Kolsky bar at a stand-off $S = 150\,\text{mm}$. The time t for each image is also included with time $t = 0$ corresponding to the instant that the striker impacts the piston.